Mon. Not. R. Astron. Soc. **302,** 549–560 (1999)

Infrared line-profile variability in Wolf–Rayet binary systems

Ian R. Stevens[1] and Ian D. Howarth[2]
[1]*School of Physics and Astronomy, University of Birmingham, Edgbaston, Birmingham B15 2TT*
[2]*Department of Physics and Astronomy, University College London, Gower Street, London WC1E 6BT*

Accepted 1998 September 17. Received 1998 September 17; in original form 1998 June 17

ABSTRACT

We present phase-resolved spectroscopy of the He I 1.0830-μm line in six Wolf–Rayet systems (WR 113 = CV Ser; WR 136 = HD 192163; WR 139 = V444 Cyg; WR 141 = HD 193928; WR 153 = GP Cep; and WR 155 = CQ Cep). Five of these systems are known WR+O binaries, with periods ranging from 1.6 d to nearly 30 d; WR 136 is only suspected of binarity. We find that the He I 1.0830-μm line profile varies systematically with orbital phase, in a qualitatively similar manner for all systems (except WR 136).

We interpret this variability as being a consequence of wind–wind interaction (i.e. colliding winds), and present results from simple models which include the effects of binary rotation and emission from the interaction region in a schematic manner. We find that the model qualitatively explains many (though not all) characteristics of the observed variability, with the shock emission an important feature; we thereby demonstrate that variability in the He I 1.0830-μm line is a sensitive indicator of wind dynamics in these colliding-wind systems.

Key words: line: profiles – binaries: close – stars: mass-loss – stars: Wolf–Rayet – infrared: stars.

1 INTRODUCTION

The general characteristics of colliding stellar winds in early-type binaries were anticipated before the discovery of any concrete observational evidence for wind–wind interaction (see, e.g., Cherepashchuk 1976 and Prilutskii & Usov 1976). However, in recent years there has been a veritable flood of observational evidence for colliding winds, particularly in Wolf–Rayet (WR) + O-star binaries. For example, at X-ray energies, observations with *EXOSAT*, *ROSAT* and *ASCA* have discovered emission from hot shocked gas at the wind–wind interface (Williams et al. 1990; Willis, Schild & Stevens 1995; Corcoran et al. 1996); in the ultraviolet, *IUE* observations have found evidence of line-profile variability in a range of systems, which has been interpreted as evidence of colliding winds (Stevens 1993; St-Louis, Willis & Stevens 1993b); at optical wavelengths, there is copious evidence for variability caused by colliding winds, in a large number of systems (e.g. Lewis et al. 1993); at IR wavelengths, the thermal emission resulting from the episodic formation of dust is believed to be associated with long-period WR + O-star binaries (Williams et al. 1992); and at radio frequencies, non-thermal emission seems to be an indicator of colliding-wind phenomena (Williams et al. 1997). In this paper we report on 1-μm spectroscopy of six Wolf–Rayet systems, and discuss profile variability in the He I 1.0830-μm line in the context of the colliding-wind paradigm.

The helium spectrum is particularly useful in determining such Wolf–Rayet parameters as radius, temperature, and mass-loss rate (e.g. Schmutz, Hamann & Wessolowski 1989), but suffers from the difficulty of finding suitable neutral-helium lines. The λ1.0830-μm ($2s\ ^3S - 2p\ ^3P^o$) triplet is valuable in this context, being the strongest He I feature in the wavelength decade ∼0.1–1 μm, and being free from serious blending. The strength and relative isolation of this line also makes it attractive for investigating orbital variability in WR binaries; more importantly, while the bulk of He II and metal-line emission is typically formed at $\sim 1-10R_*$ (where R_* is a characteristic radius of the quasi-hydrostatic core; cf., e.g., Schmutz et al. 1989), λ1.0830 μm arises at radii which are several times larger. For binary systems with periods of order a few days, this brings the line-forming volume into coincidence with the scale of structures associated with colliding winds (of the order of the binary separation and larger), suggesting that the He I spectrum should be an especially useful diagnostic of such structures.

Previous observations of He I 1.0830-μm have been presented by Williams & Eenens (1989), Vreux, Andrillat & Biémont (1990), Howarth & Schmutz (1992) and Eenens & Williams (1994), all of whom discussed single (or a few) observations of moderate numbers of WR stars. In the present paper we have followed a substantially different approach, obtaining multiple observations of a small number of close binary systems. Variations in the He I 1.0830-μm line were already hinted at in observations reported by Howarth & Schmutz (1992), but in this paper we extend the orbital phase coverage substantially, in order to determine the nature of variability in a small number of targets. As we will show, this variability can be very marked and, in the light of the modelling work presented in Section 4, appears to be an excellent probe of the wind dynamics in colliding-wind systems.

The paper is organized as follows. In Section 2 we describe the observations; in Section 3 we discuss the characteristics of the data

Table 1. Details of the target stars. The WR catalogue numbers and stellar data are from the compilations by van der Hucht *et al.* (1988 and in preparation); the final column gives the number of He I 1.0830-μm observations.

WR No.	Name		Spectral Type	P_{orb} (days)	Distance (kpc)	v	$E(b-v)$	No. of Obs.
WR 113	CV Ser	HD 168206	WC8+O8–9IV	29.71	2.0	9.5	0.81	7
WR 136	V1770 Cyg	HD 192163	WN6b(h)+ ?	4.55	1.8	7.6	0.33	5
WR 139	V444 Cyg	HD 193576	WN5o+O6	4.21	1.7	8.2	0.71	25
WR 141	–	HD 193928	WN5o+OB	21.69	1.8	10.1	1.05	4
WR 153	GP Cep	HD 211853	WN6o/WCE+O6I	6.69	3.5	9.1	0.56	13
WR 155	CQ Cep	HD 214419	WN6o+O9Ib–II	1.64	3.5	8.8	0.53	15

Table 2. Log of observations; phases are computed using the ephemerides given in Section 3, and in each case phase zero corresponds to conjunction with the WR component being the closer to the observer.

JD mid-exp. −2 448 000	(cycle).phase	JD mid-exp. −2 448 000	(cycle).phase	JD mid-exp. −2 448 000	(cycle).phase
WR 113 (CV Ser)		WR 136 (HD 192163)		WR 139 (V444 Cyg)	
111.420	(158).596	111.405	(553).796	111.390	(80).169
114.397	(158).697	113.363	(554).226	112.490	(80).431
115.505	(158).734	820.719	(709).689	112.681	(80).476
821.412	(182).496	825.561	(710).753	113.393	(80).645
825.385	(182).630	828.538	(711).408	113.662	(80).709
828.488	(182).734			114.364	(80).876
828.503	(182).735	WR 141 (HD 193928)		114.555	(80).921
		112.539	($\overline{33}$).402	114.706	(80).957
WR 155 (CQ Cep)		821.441	(0).086	115.429	(81).128
111.516	(20174).401	825.593	(0).278	115.623	(81).174
112.712	(20175).129	828.570	(0).415	116.400	(81).359
115.683	(20176).940			820.663	(248).545
820.736	(20606).523	WR 153 (GP Cep)		821.389	(248).717
821.492	(20606).984	111.609	(661).038	821.662	(248).782
821.644	(20607).078	115.655	(661).643	822.565	(248).996
822.613	(20607).668	820.691	(767).055	822.590	(249).002
823.488	(20608).201	821.510	(767).178	823.416	(249).198
823.662	(20608).307	822.630	(767).345	823.642	(249).252
824.540	(20608).842	823.465	(767).470	824.417	(249).436
824.685	(20608).930	823.676	(767).501	824.669	(249).496
825.635	(20609).510	824.518	(767).627	824.604	(249).480
826.485	(20610).027	824.728	(767).659	825.574	(249).711
827.488	(20610).639	825.611	(767).791	826.410	(249).909
828.708	(20611).382	826.459	(767).917	827.668	(250).208
		827.508	(768).074	828.550	(250).417
		828.724	(768).256		

and present a brief analysis of the results; and in Section 4 we describe a simple colliding-wind model, which can be used to understand many aspects of the observed variability in these systems.

2 OBSERVATIONS

The observations were all taken with the 2.5-m Isaac Newton Telescope; the principal data set was obtained during 1992 July 17–25, but we have included a number of observations obtained during 1990 August 7–12 with a similar set-up (cf. Howarth & Schmutz 1992). Spectra were obtained by using the Intermediate Dispersion Spectrograph and R600I grating, with a 23.5-cm camera and an EEV CCD (1280 × 1180 22-μm pixels), giving a reciprocal dispersion of 23 Å mm^{-1} (1.6 Å pixel^{-1}; $R \simeq 3400$). Although the EEV chip, in common with all optical CCDs, had a plummeting response at 1 μm, it had the considerable advantage of being almost completely free of fringing problems; the chip was also run slightly warm to improve far-red response. The data were bias-corrected, flat-fielded, interactively corrected for cosmic ray events, and optimally extracted with the Starlink FIGARO and ECHOMOP packages (Shortridge et al. 1997; Mills, Webb & Clayton 1997); subsequent manipulation of the spectra was carried out principally with DIPSO (Howarth et al. 1996).

We concentrated our attention on three short-period WR + O-star binaries (V444 Cyg, GP Cep and CQ Cep) with orbital periods, P_{orb}, ranging from 1.6 to 6.7 d. In addition, we obtained a smaller number of observations of two longer period systems: CV Ser (a WC binary with $P_{orb} = 29.7$ d) and HD 193928 (a WN6 + O-star binary with $P_{orb} = 21.7$ d). We also made a few observations of the suspected WR binary HD 192163. Some relevant astrophysical parameters for each of the six targets are summarized in Table 1, and a log of the observations is given in Table 2. All integrations were in the range 900–1800 s, i.e., much shorter than the orbital periods.

3 SPECTROSCOPIC RESULTS

3.1 WR 113 (CV Ser, HD 168206)

CV Ser, the only WC system in our sample, is a double-lined

spectroscopic binary with a period of 29.7 d. Hjellming & Hiltner (1963) reported a 0.5-mag deep eclipse that has not been re-observed, and is now believed to be an isolated (and mysterious) event. However, CV Ser does show 'wind' eclipses (Howarth, Willis & Stickland 1982; St-Louis et al. 1993b). Only a weak upper limit on the X-ray emission is available, from the *ROSAT* All-Sky Survey: $L_X \leq 4.5 \times 10^{31}$ erg s^{-1} (Pollock, Haberl & Corcoran 1995). We adopt the following orbital ephemeris:

$$\phi = 2443\,400.0 + 29.707E \quad (1)$$

(Massey & Niemela 1981). Here phase zero corresponds to the WR component in front, a convention we generally adopt in this paper; the uncertainty in the predicted phases at the time of our observations is $\lesssim 0.03$.

The He I 1.0830-μm observations are shown in Fig. 1(a). The relatively long period of the system, together with unfortunate phase sampling, means that our orbital coverage is very incomplete, but the observations show a general mode of variability which is consistent with that observed in systems where we have better phase coverage, particularly WR 139 (Section 3.3). The main features are (i) the P Cygni absorption dip is weaker at $\phi \sim 0.6$ than at adjacent phases, and (ii) the general shape of the profile changes with phase, with the redshifted portion becoming increasingly important after $\phi \simeq 0.5$.

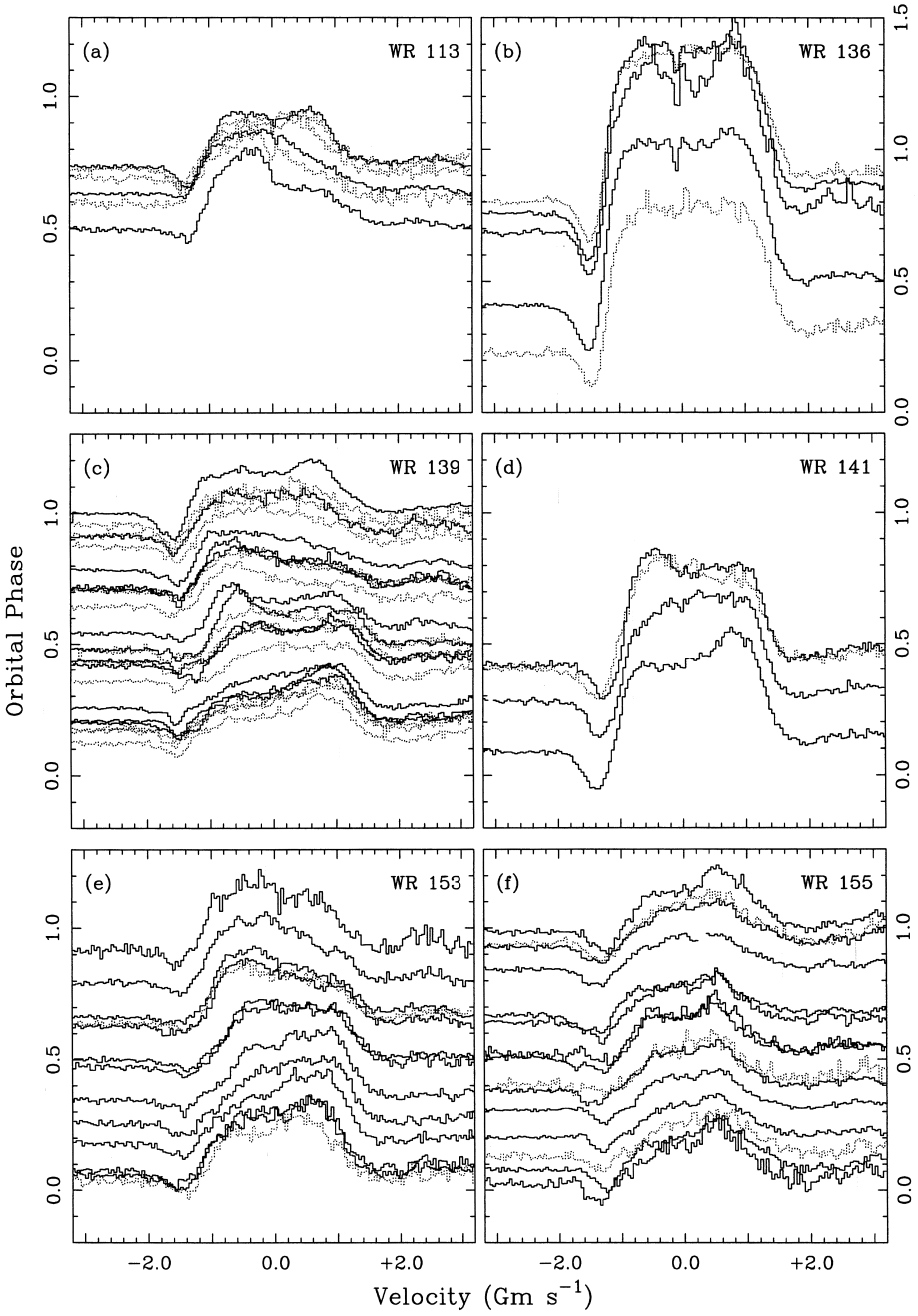

Figure 1. Observations of He I 1.0830-μm. Spectra obtained in 1992 are plotted with solid lines, and those from 1990 with dotted lines. Each spectrum is vertically offset such that the continuum level is at the appropriate orbital phase; the zero level for each spectrum is at a point corresponding to a phase 0.2 smaller. Phase zero is defined as conjunction with the WR star in front.

3.2 WR 136 (HD 192163)

HD 192163 is a prototypical WN6 star which has been suspected of being in a 4.6-d orbit, possibly with a neutron-star companion (Koenigsberger, Firmani & Bisiacchi 1980; Aslanov & Cherepashchuk 1981). St-Louis et al. (1989) report UV variability on a ~1-d time-scale, but not repeating on the mooted binary period; the system's low X-ray luminosity, $L_X \sim 2\times10^{31}$ erg s^{-1} (Wrigge, Wendker & Wisotski 1994; Pollock et al. 1995), also argues against an accreting neutron-star companion. There have been suggestions of a shorter 0.45-d period (Vreux, Andrillat & Gosset 1985), but the reality of this period has been questioned by Matthews & Beech (1987).

The status of HD 192163 is therefore unclear, although the evidence for binarity is rather weak. We obtained five He I 1.0830-μm observations to see if this system shows the same variability as the other WN + O-star binary systems. The data are shown in Fig. 1(b), phased according to

$$\phi = 2445\,591.633 + 4.55E \qquad (2)$$

(St-Louis et al. 1989). Our data show little sign of any gross systematic variability or profile asymmetry. This is in contrast to all the well-established WR + O binaries we observed, suggesting that colliding-wind effects are unimportant in this system on the time-scales we have sampled. There is, however, some evidence for variable subpeak structure in our data, probably associated with stochastic small-scale structure in the outflow (cf. Robert 1994).

3.3 WR 139 (V444 Cyg)

V444 Cyg is the brightest disc-eclipsing WR+O-star binary, and as such is of key importance in understanding colliding-wind phenomena, first inferred in this system from UV line-profile variability by Shore & Brown (1988). Among numerous other studies, optical photopolarimetry has been presented by St-Louis et al. (1993a) and spectropolarimetry by Harries, Hillier & Howarth (1998). X-ray observations (Corcoran et al. 1996) indicate a luminosity of $L_X \sim (4-9)\times10^{32}$ erg s^{-1}. The recent detailed studies of optical line-profile variability by Marchenko, Moffat & Koenigsberger (1994) and Marchenko et al. (1997) are of particular bearing on the present investigation.

The orbital ephemeris we adopt is from Underhill, Grieve & Louth (1990):

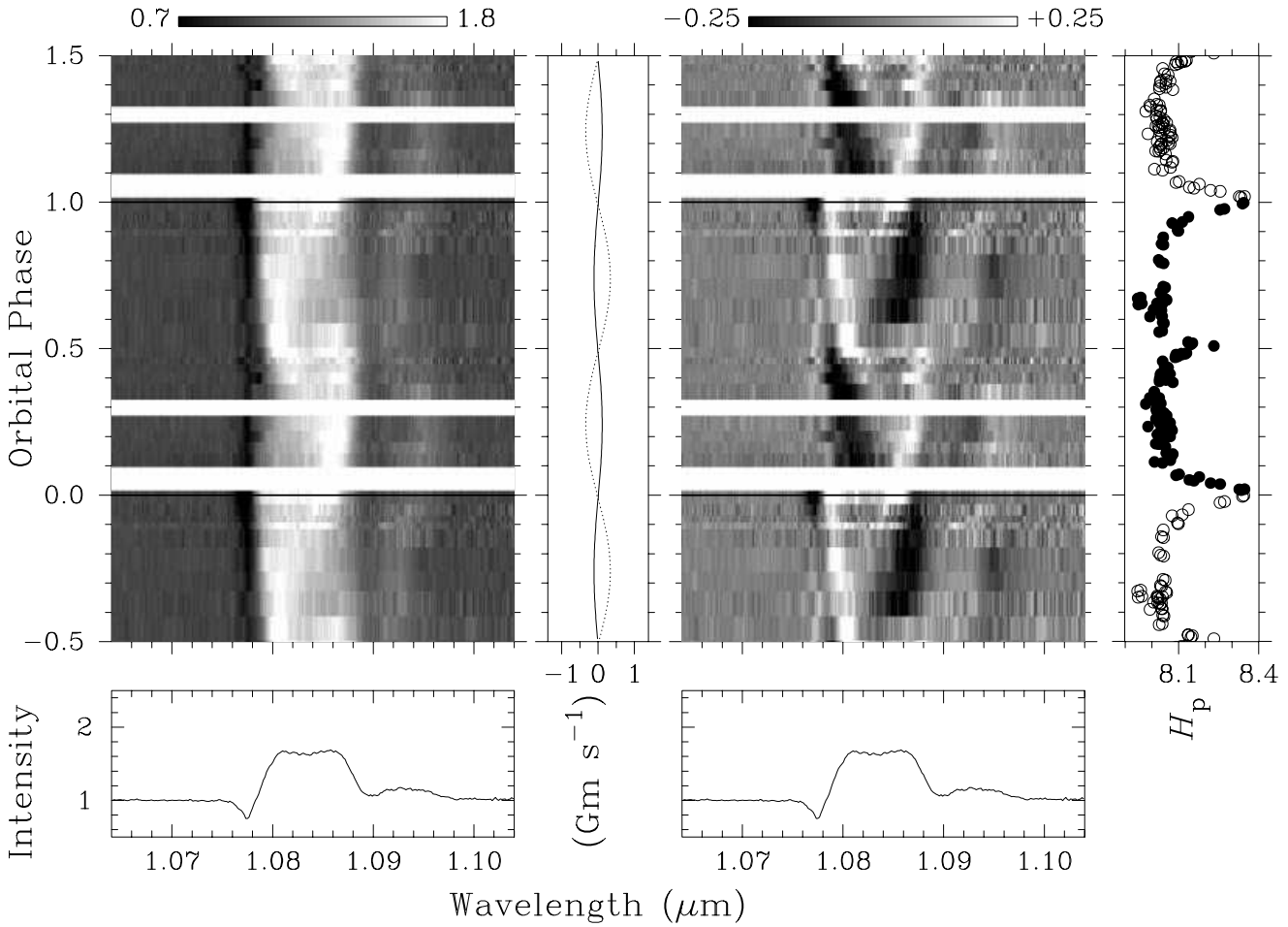

Figure 2. Dynamic spectra for V444 Cyg, displayed over two complete orbital cycles. The left-hand grey-scale shows directly the observed variability in He I 1.0830 μm, while the right-hand grey-scale shows the difference spectra, following subtraction of the mean spectrum (reproduced in the lower two panels). Both panels have been constructed using observer's-frame velocities; observations separated by less than 0.01 in phase have been averaged, and blank regions correspond to gaps in phase coverage greater than 0.1. The weak feature at ~1.093 μm is due to blended He II (12–6) and H Pγ. The central panel shows the orbital centre-of-mass velocity variations of the WR and O-type components (solid and dashed lines, respectively) according to Underhill, Yang & Hill (1988), on the same abscissal scale as the grey-scales. The right-hand panel shows the *Hipparcos* photometry (ESA 1997), which is roughly contemporaneous with our spectroscopy, to illustrate general pattern of continuum variability.

$$\text{HJD (pri.min.)} = 2447\,773.68 + 4.21245E, \quad (3)$$

where phase zero corresponds to eclipse of the primary (O-type) star. The orbital period of V444 Cyg is increasing because of angular momentum redistribution consequent on mass-loss from the WR star; published values for the rate of change of period range from $\dot{P} = 0.088$ to 0.222 s yr^{-1} (Khaliullin, Khaliullina & Cherepashchuk 1984; Underhill et al. 1990), but the consequences of these differences for the phases given in Table 2 are negligible.

The phase-folded He I 1.0830-μm spectra for V444 Cyg are shown in Fig. 1(c). The mean spectrum is flat-topped (a common characteristic of He I 1.0830 μm in W-R stars), but substantial, phase-dependent variability is evident; at $\phi \simeq 0.1$–0.4 the line profile slopes down to the blue, while at phases $\phi \simeq 0.6$–0.9 the reverse is true. In addition to this systematic variation, there is evidence for a short-lived 'spike' which appears in the blue side of the emission shortly after $\phi \simeq 0.5$ (with a possible counterpart in the red side just after $\phi \simeq 0.0$). The strength of the absorption component is also variable, almost disappearing at phases around $\phi \simeq 0.5$–0.6 and deepening at phases $\phi \simeq 0.9$–0.1. As can be seen in Fig. 1(c), this behaviour reproduces well over a baseline of 2 yr (~170 orbital cycles), as well as through the two separate cycles covered in each of 1990 and 1992.

The same data are shown in grey-scale format in Fig. 2. In this representation, the raw data (left-hand panel) clearly show a dominant 'S-wave' variation in the emission line. This pattern is also evident in the difference spectra (right-hand panel), which reveal further complexity, particularly in the form of high-velocity emission receding from the observer at phases ~0.2–0.5 and approaching at phases ~0.7–1.0.

3.4 WR 141 (HD 193928)

HD 193928 is a WN5 system with a O4–5 companion; orbital phases are given by

$$\phi = 2448\,819.57 + 21.6895E \quad (4)$$

(Marchenko, personal communication), where phase zero again corresponds to inferior conjunction of the WR component. Photometric variations have been detected, but appear to repeat on a different period (Marchenko et al. 1998). WR 141 has received little attention in recent years (cf. Grandchamps & Moffat 1991), but has been marginally detected at X-ray energies ($L_X \sim 2 \times 10^{31}$ erg s^{-1}; Pollock et al. 1995).

The spectra are shown in Fig. 1(d). Although our sampling is very sparse, and the period longer than our observing runs, large-amplitude changes are evident, and appear to be broadly similar in nature to those seen in other stars, and especially WR 139. The absorption component appears somewhat weaker at phase 0.4, as can also be seen in Fig. 5, and the emission peak moves from red to blue between phases 0.1 and 0.4. Given the large amplitude of the line-profile changes, this star would probably repay further study.

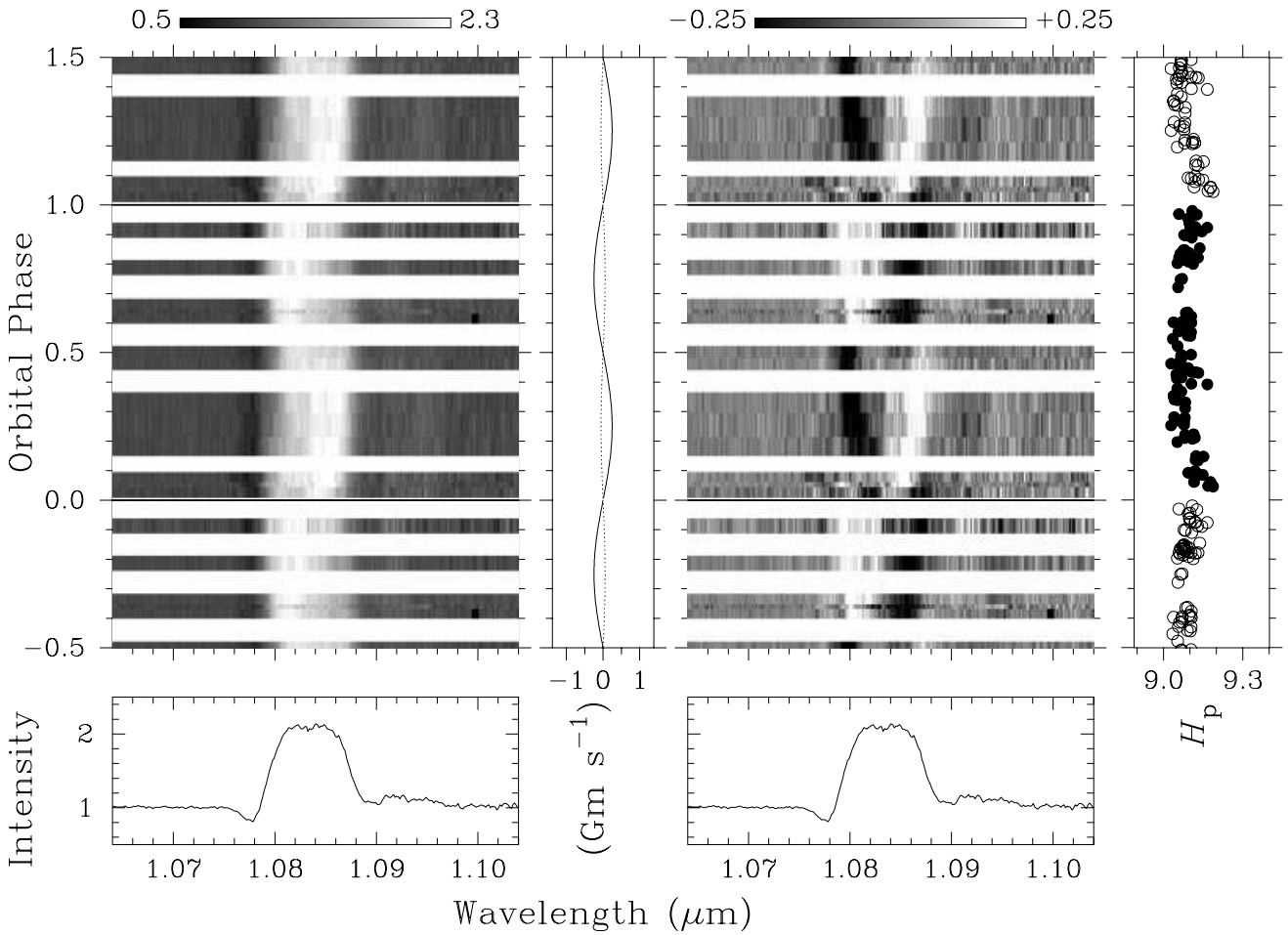

Figure 3. Dynamic spectra for WR 153/GP Cep; details are as in Fig. 2.

3.5 WR 153 (GP Cep, HD 211853)

GP Cep is a complex system, first studied by Wilson (1940) and Hiltner (1945). Massey (1981) showed the system to be quadruple, consisting of two early-type short-period binaries: one a WR + O-star system with a period of around 6.7 d, and the other an O + O-star binary with a 3.5-d period (see also Massey & Grove 1989). Panov & Seggewiss (1990) confirm this general picture, except that they conclude that both systems are WR+O-star binaries. Although GP Cep exhibits both WN and WC spectral characteristics, Massey & Grove show that the C IV λ5806 and N IV λ7107 lines vary in phase, and therefore originate in a single Wolf–Rayet, classified WNC. GP Cep has been detected as an X-ray source, with $L_X \sim 4 \times 10^{32}$ erg s^{-1} (Pollock et al. 1995).

We have phased our observations against both short-period ephemerides; the results shown in Figs 1(e) and 3 are ordered according to the ephemeris for the dominant WNC + O system,

$$\text{HJD (pri.min.)} = 2443\,690.32 + 6.6884E \quad (5)$$

(Massey 1981); the phases are expected to be good to ~0.01 at the time of our observations. It is clear once again that there is systematic variability, which is very similar to that seen in WR 139. The main feature are: (i) the overall shape of the emission profile changes, with the red side of the emission stronger at phases 0.1–0.4, and the blue side stronger at $\phi = 0.6$–0.9; and (ii) the absorption profile weakens markedly at phases around 0.6.

3.6 WR 155 (CQ Cep, HD 214419)

This well-studied system has the shortest orbital period of any of the known binaries in the sample. It is an eclipsing system, with primary minimum ($\phi = 0.0$) corresponding to eclipse of the O-star primary by the WR component. Phases have been calculated from

$$\text{HJD (pri.min.)} = 2415\,000.410 + 1.6412436E \quad (6)$$

(Walker et al. 1983). Even though some 20 000 orbital cycles had elapsed between the fiducial epoch of this ephemeris and our observations, the phasing is good to ~0.01 (cf. Harries & Hilditch 1997 and the photometry shown in Fig. 4).

Stickland et al. (1984), Marchenko et al. (1995) and Harries & Hilditch (1997), among others, have presented detailed studies of CQ Cep. CQ Cep is at best marginally detected as an X-ray source, with a very low X-ray luminosity ($L_X \sim 5 \times 10^{30}$ erg s^{-1}; Pollock et al. 1995). There is some evidence of a period decrease with $\dot{P} \simeq -0.019$ s yr^{-1} (Cherepashchuk 1982; see also Kilinç 1994), although Walker et al. (1983) question its reality. If the period *is* decreasing, then this would suggest mass transfer from the (more massive) WR component on to the O star, in addition to the wind mass-loss that is presumably occurring from both stars in the system. In practice, this period change has negligible effect for our purposes.

Our spectra are shown in Figs 1(f) and 4. The He I 1.0830-μm

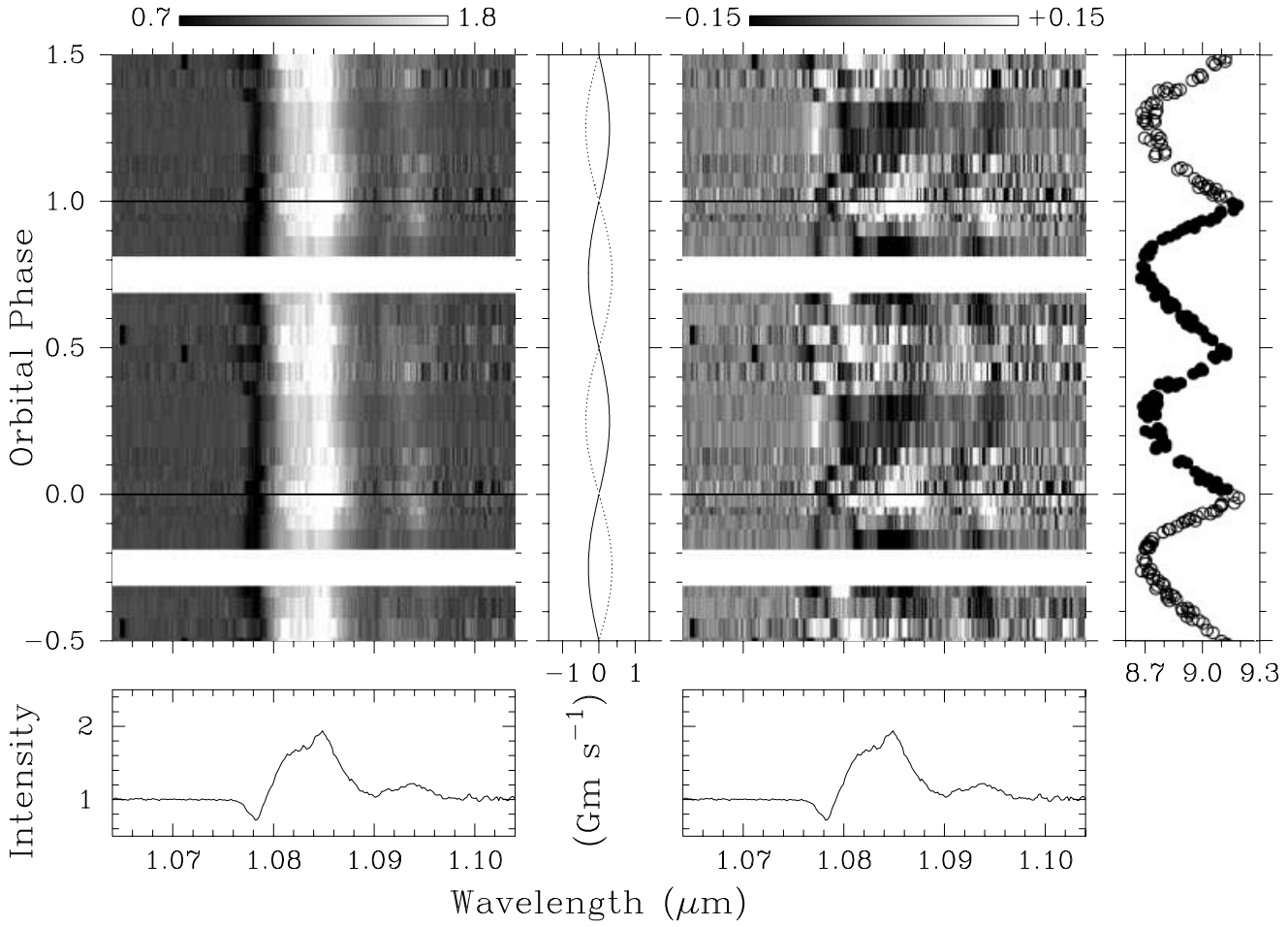

Figure 4. Dynamic spectra for WR 155/CQ Cep; details are as in Fig. 2.

feature shows a persistent asymmetry, with a redwards emission peak throughout the orbit, and rather smaller variations than observed in several of our other targets. When the individual spectra are differenced with their mean, however, there is some evidence of a pattern of variability which appears to be roughly consistent with that seen in other stars (cf. Fig. 4 and Section 3.7). Also, although there seem to be significant orbit-to-orbit changes, it is clear that the absorption profile again largely disappears around $\phi \simeq 0.6$.

3.7 Summary of observations

As is evident from the foregoing, considerable line-profile variability is present in all the well-established binary systems. Not only do the gross characteristics of this variability reproduce from orbit to orbit in a given star, but also the nature of the variability appears to be broadly similar from one star to another (cf. Fig. 1), with the peak of the emission profile 'swaying' from blue to red, such that the grey-scales (Figs 2 and 3) can be interpreted as basically showing a distorted S-wave. (Although the velocity shifts of the line centroid follow the general trend of the orbital motion of the WR component, simple Keplerian motion is evidently not the sole cause of those shifts, as their amplitude greatly exceeds that of the centre of mass; cf. Figs 2–4.)

To quantify these results, we present measurements of the equivalent widths, W_λ, in Fig. 5. The behaviour of the absorption component for each of the well-observed systems V444 Cyg, GP Cep, and CQ Cep is broadly similar, with maxima in the equivalent widths near phase zero and minima close to phase 0.5 (when the O star is in front of the WR star). The emission components are much less variable, but show a peak in W_λ for V444 Cyg and CQ Cep around $\phi \simeq 0.0$, with probable secondary maxima around $\phi = 0.5$. However, this equivalent-width variation is *entirely* consistent with the reflex response of a constant-flux line to the continuum-level changes illustrated in Figs 2–4. Thus the morphological changes we observe are not accompanied by significant changes in emission flux.

As a simple indicator of the 'swaying' behaviour evident in the line profiles, we define an asymmetry parameter, $W_\lambda(V)/W_\lambda(R)$, where $W_\lambda(V)$ [(R)] is the emission equivalent width to the violet [red] of zero velocity; Fig. 6 shows the results. This parameter clarifies the low-amplitude variability in CQ Cep, which is now revealed to be qualitatively very similar to that for the other well-observed systems, V444 Cyg and GP Cep: red wing stronger at $\phi \simeq 0.2$, and blue wing stronger at $\phi \simeq 0.7$.

4 A COLLIDING-WIND MODEL

In the previous sections we have summarized observations that

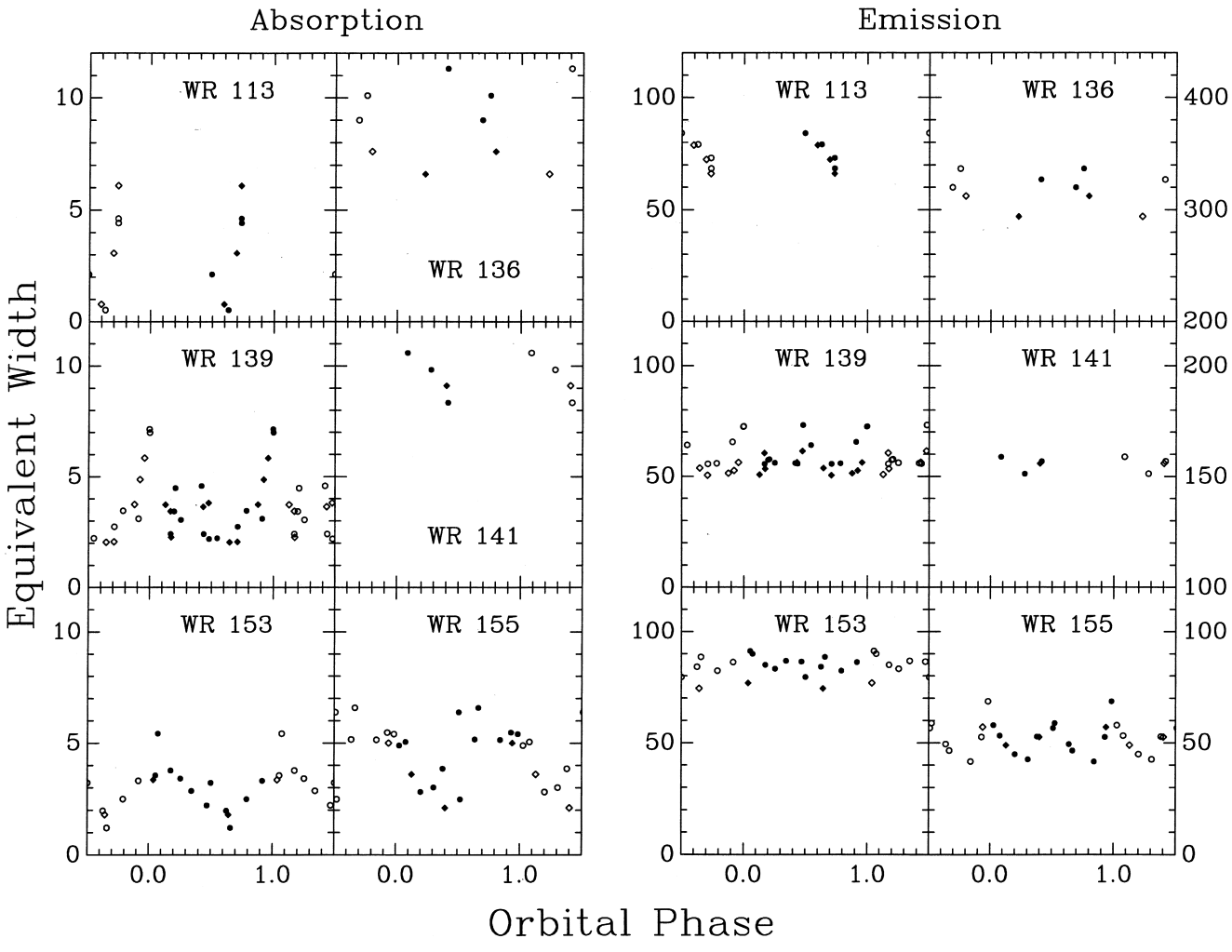

Figure 5. Equivalent-width variations, in Å (absorption) or −Å (emission), plotted over two orbital cycles; diamonds are from 1990 observations, and circles from 1992. The variations in equivalent width for WRs 139 and 155 are consistent with a constant line flux, moderated by continuum variability.

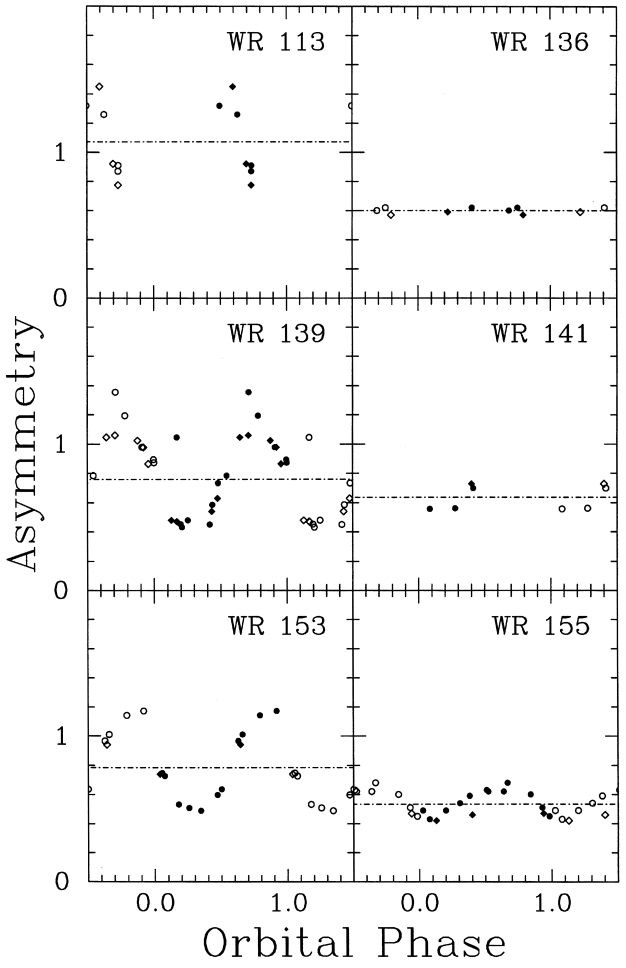

Figure 6. Asymmetry parameter (cf. Section 3.7); horizontal dashed lines show mean values for each star, and larger-than-average values correspond to the blue wing being favoured. The well-observed systems WR 139, WR 153 and WR 155 (and possibly also WRs 113 and 141) show the same general trends.

Table 3. Parameters for model calculations. (These parameters correspond approximately to the V444 Cyg system.)

Parameter	WR star	O-star
$\dot{M}$ ($M_\odot$ yr^{-1})	1.4×10^{-5}	3.0×10^{-6}
v_∞ (km s^{-1})	1500	3000
R_* ($R_\odot$)	3.0	10.0
Binary separation	40 $R_\odot$	
Orbital inclination	90°	

show a consistent picture of line-profile variability in a range of WR + O-star systems, and it seems inevitable that the observed variability is related to binarity. We now present simple models of this variability, which indicate that the observed behaviour can largely be understood as a consequence of colliding stellar winds.

Our modelling of line-profile variations concentrates on a region of parameter space roughly appropriate to our best-observed system, V444 Cyg; the binary and stellar parameters we adopt are listed in Table 3 (cf. Shore & Brown 1988). We will develop the model in a stepwise manner to illustrate the effects of various ingredients on the line profiles; this model has several similarities to that presented by Lührs (1995) to explain the variable double-peaked structure seen in the C III λ5696 line of the WC + O-star binary WR 79.

4.1 The basic model

Our models assume a binary system consisting of a WR and an O-type star in a circular orbit, with radii R_*(WR), R_*(O), mass-loss rates $\dot{M}$(WR), $\dot{M}$(O), and terminal velocities v_∞(WR), v_∞(O). The winds are assumed to accelerate as

$$v(r) = v_\infty\left(1-\frac{R_*}{r}\right)^\beta, \tag{7}$$

with $\beta \simeq 1$.

There are two principal sites of emission that are important in any model of spectroscopic behaviour in WR + O colliding-wind systems. One is the wind–wind interface, a region of locally dense gas, which we will consider in Section 4.3. The other is the distributed He I 1.0830-μm emission, which we assume originates entirely in the WR wind, with a negligible contribution from the O-star wind. This is a reasonable assumption considering the helium densities in the two winds, and is supported by direct observations of the He I 1.0830-μm line in isolated WR and OB stars (Howarth & Schmutz 1992; Conti & Howarth 1998).

The geometry of the distributed emission is determined by the outflow from the WR star, moderated by a 'cavity' swept out by the O-star wind. The extent of this cavity is largely determined by the wind momentum ratio,

$$\mathcal{R} = \left[\frac{\dot{M}(\mathrm{WR})\,v_\infty(\mathrm{WR})}{\dot{M}(\mathrm{O})\,v_\infty(\mathrm{O})}\right]^{1/2} \tag{8}$$

(Stevens, Blondin & Pollock 1992). The line-profile variability thus depends primarily on the value of $\mathcal{R}$, rather than on the individual stellar-wind parameters, such as mass-loss rates and terminal velocities. The parameters listed in Table 3 were chosen to give a fairly low value of $\mathcal{R}$ (∼1.5), resulting in a relatively wide opening angle for the O-star wind (in agreement with the empirical estimate for V444 Cyg by Marchenko et al. 1994), and hence a relatively large degree of variability.

The detailed shape of the cavity is determined by the interaction surface of the two winds, which is, in turn, essentially given by equating the momentum fluxes of the two winds perpendicular to that surface (see Luo, McCray & Mac Low 1990 and Stevens et al. 1992 for full details). For our basic model we perform this calculation assuming symmetry about the line of centres, i.e., ignoring orbital motion.

With the binary and wind geometries specified, the line profile is determined by the emissivity of He I 1.0830 μm, and the radiative transfer. Although calculations of the radial distribution of emission are available for single stars (e.g. Hillier 1987), the line-formation physics in binary systems will be different for a number of reasons.

(i) Different radiation field – the O star in most of these systems is comparable in luminosity to the WR star, and will change the ionization structure through a large volume of the wind (cf. Hamann & Schwarz 1992). Even with a fixed dynamical structure, this will affect the line emissivity.

(ii) X-ray emission from the wind–wind shock will also impact on the ionization structure in the interaction zone. Some attempt has been made to investigate the effect of X-rays on the wind structure of the single O star ζ Pup by Hillier et al. (1993); in the case of colliding winds we might expect the effects to be greater because of

the higher level of X-ray emission generated by the wind–wind collision. Hillier et al. (1993) make the point that in the case of a single O star only a small fraction of the emitted X-ray emission actually escapes the system; the rest is absorbed by the wind. Such a situation will, in general, also be true in colliding winds.

(iii) The changes in the radiation field and ionization structure compared to the single-star case, together with the direct gravitational effects of the O star, will alter the velocity structure of the WR-star wind (Stevens & Pollock 1994; Gayley, Owocki & Cranmer 1997). Changes in the velocity structure will be directly reflected in the large-scale density structure.

Although calculations of these effects could be made, in principle, for a qualitative investigation of large-scale effects, we have chosen a simple analytical function for the He I 1.0830-μm emission, which we assume to be uniform (per unit volume) at radii 20–140 $R_\odot$ in the WR wind, and negligible elsewhere (cf. Lewis et al. 1993). In view of this approximation, we elected to treat the emission simply as optically thin, which is consistent with the observed constant level of line flux. (An important consequence of this simplification is that we cannot directly model P Cygni absorption.) Given these gross simplifying assumptions our results should be treated as being largely schematic, but they none the less prove to be useful in investigating the role of colliding winds in the line-profile changes.

Having established a prescription for the dynamics and emissivity of the winds, we calculate the location of the wind interaction surface and construct a 3D model of the colliding-wind system

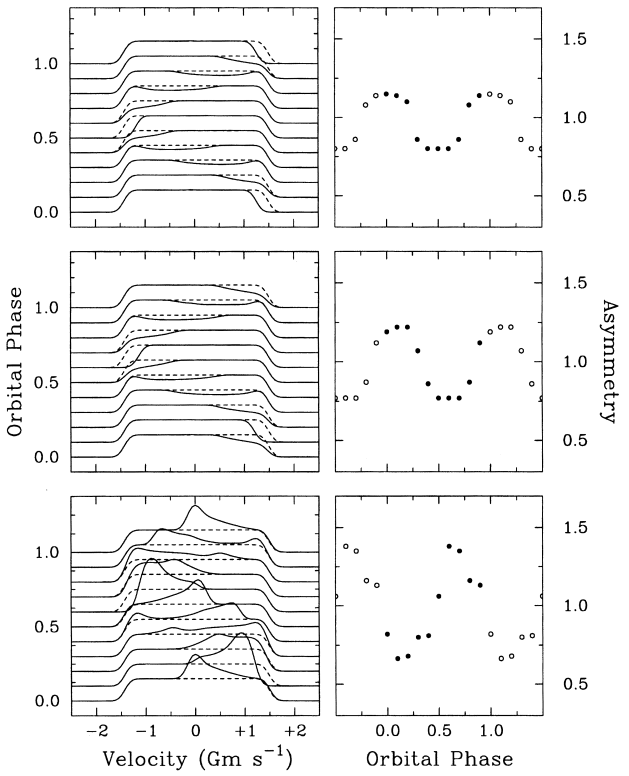

Figure 7. Synthetic He I 1.0830-μm data. The left-hand panels show the orbital line-profile variability, and the right-hand panels the corresponding asymmetry parameters (cf. Section 3.7); the dashed line shows the profile predicted in the absence of a binary companion. Top: a model assuming no binary rotation and no emission from the wind-shock. Middle: including binary rotation, but no emission from the shock. Bottom: including binary rotation and emission from the wind–wind interface.

(typically on a 400^3 grid), initially assuming rotational symmetry around the binary line of centres. Each grid point is assigned to the wind of the WR or O star, and a corresponding outflow velocity obtained from equation (7). The emission contributions from each grid point are then summed according to projected velocity for a given binary phase, accounting for occultation effects, to generate a model line profile.

Results from this basic model of colliding-wind variability are shown in the upper left panel of Fig. 7. The cylindrical symmetry of the emission cavity means that variability is symmetric about phase $\phi = 0$; thus, while this simple model can clearly generate phase-dependent line-profile variability, the phase dependence is rather different from that observed. Essentially, we see a drop in emission which tracks the projected velocity of the He I cavity around the O star: thus, at $\phi = 0$, the line profile is truncated at extreme redshifted velocities, while at quadratures the line centre is depressed. A plot of the asymmetry parameter for this model (top right panel of Fig. 7) reflects this, showing a roughly sinusoidal variation, but, in accord with the line-profile changes, is smallest (i.e., blue wing weakest) at $\phi = 0.5$.

The amplitude of the model variability can be modified by changing the opening angle of the O-star wind (through altering $\mathcal{R}$), but to affect the basic phase dependence requires consideration of additional factors. For V444 Cyg and GP Cep the observed minimum in the asymmetry parameter is at $\phi \simeq 0.3$–0.4; the need for a corresponding phase shift in the model suggests that we drop the assumption of cylindrical symmetry.

4.2 Binary rotation

In order to introduce phase shifts indicated by the observations, we first consider the 'winding-up' of the wind–wind interface which must result from orbital motion. In the spirit of our previous approximations, we include orbital motion in a rather ad hoc manner, by simply rotating the shock surface by an angle δ about the O star. In reality, we expect a more complex (~spiral) geometry, but for the parameters of Table 3 the flow time across the binary separation is only ~4 h, so our approach is not unreasonable for the inner parts of the system, which we expect to dominate the line formation.

Straightforward dynamical considerations suggest

$$\delta \simeq \tan^{-1}\left(\frac{v_{\rm orb}}{v_{\rm wind}}\right) \qquad (9)$$

as a reasonable approximation to the angular deflection at the orbit of the O-type star, where $v_{\rm wind}$ is the WR wind velocity at the binary separation, and $v_{\rm orb}$ the orbital velocity of the O star; for V444 Cyg we have $v_{\rm orb} \simeq 480$ km s^{-1}, whence $\delta \sim 20°$. Because the shock surface falls progressively further behind the orbiting O star, this angle increases with increasing radial distance from the WR component. In order to illustrate clearly the effect of rotation in our simple model, we adopt $\delta = 45°$.

Results for the modified model are shown in the middle panels of Fig. 7. The effect of rotation is to introduce a phase shift of about 0.125 in the profile variability and asymmetry parameter (corresponding to the adopted 45° rotation of the shock surface). However, the shift is in the sense of *increasing* the phase of maximum asymmetry parameter – the opposite sense to that required by the observations. This forward phase shift is inescapable for any model in which the helium cavity trails the O star's orbital motion.

This model therefore also fails to explain the observations presented in Section 3. To account for the phase shift of the

asymmetry parameter, we evidently require an *emission* source associated with the wind cavity. An obvious candidate for the site of this emission is the bow shock (wind–wind interaction region) around the O star.

4.3 Bow-shock emission

The asymmetry-factor observations suggest that there is an emission *excess,* rather than a deficit, in the general vicinity of the O star; in the context of colliding-wind models, this excess is most plausibly attributed to the wind–wind interface. The gas in the interface region will initially have been shocked to high temperatures, but the post-shock density in short-period systems is sufficient to allow significant cooling (Stevens et al. 1992), with consequent He I emission. Similar effects have been reported previously in optical observations of He I lines in CX Cep (Lewis et al. 1993) and V444 Cyg (Marchenko et al. 1994, 1997).

We do not attempt a detailed model of the emission from the complex shocked region around the O star, but, in the spirit of our earlier simplifications, include it in a schematic way. We assume that the emission can be parametrized such that the flux from a particular grid point on the interface is given by

$$\text{Flux} = C\left(\frac{D_{\rm Sep}}{r}\right)^{\gamma}, \qquad (10)$$

where C is a constant, $D_{\rm Sep}$ is the binary separation, and r is the radial distance from the WR star. (This formulation ensures that the trailing edge of the interface region has more emission than the leading edge, as expected given the greater densities at the former site.) The velocity of the shocked gas is assumed to be given by the component of the pre-shock WR wind velocity perpendicular to the line of centres. Occultation and obscuration effects are included for this emission, as well as the effects of binary rotation as discussed above (to produce the required phase shifts).

Fig. 7 includes synthetic spectra for a model with shock emission calculated according to this prescription, where we used $\gamma = 2$ and adjusted the value of the arbitrary normalizing constant C in order to ensure that the effect of the shock emission on the model profiles exceeds that of the cavity in the distributed emission. The grey-scaled results are compared to observations of WR 139 in Fig. 8, and an equatorial slice through this model is shown in Fig. 9.

The characteristics of this model are easily understood. To zeroth order, we may consider the shock (emission) surface to be a cone of gas of constant flow velocity, with the axis of symmetry of the cone offset from the line of centres by an angle δ (chosen to simulate the effect of binary rotation). Any line drawn on the surface of such a cone from the apex traces material of fixed projected velocity at any given phase, and the S-wave patterns evident in Fig. 8 follow the orbital dependence of the projected velocity of the leading (fainter)

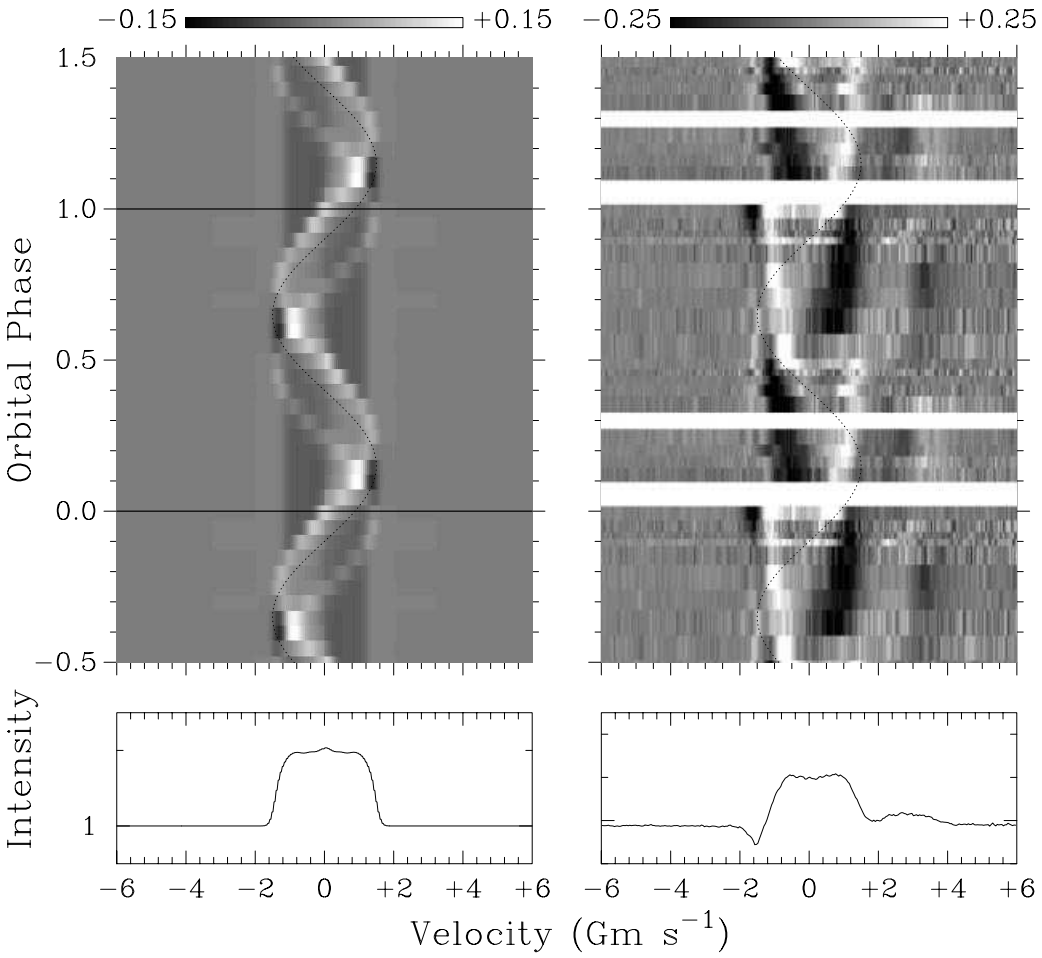

Figure 8. Left: dynamic spectrum generated from difference spectra for the 'rotation + shock' model illustrated in Fig. 9. Right: observations of WR 139 on a similar scale. A sine wave is drawn through both frames to emphasize the common 'S-wave' pattern in the emission.

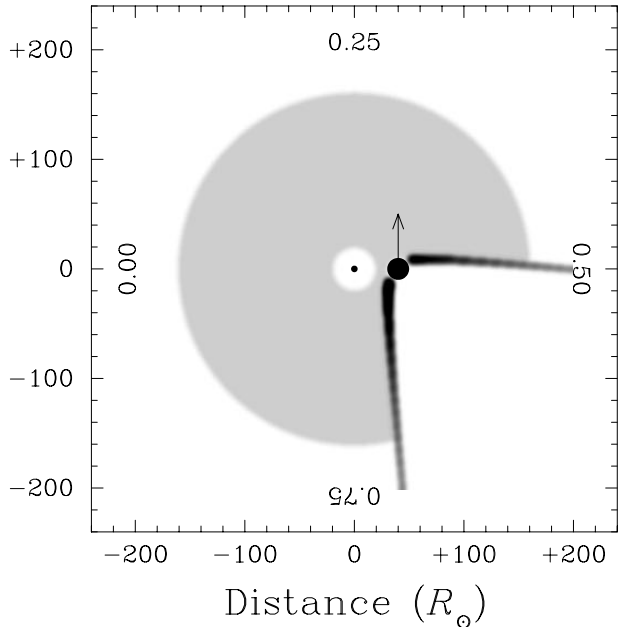

Figure 9. An equatorial slice through a model including binary rotation and shock emission, showing the locations of distributed He I emission from the WR wind and localized emission from the wind–wind interface. The arrow indicates the direction of binary motion of the O star, and viewing directions for four binary phases are indicated.

and trailing (brighter) edges of the cone. (Gas out of the orbital plane generates emission at intermediate projected velocities, of course, but that emission is inconspicuous because the average distance from the WR component is greater.) The phasing of the model S-wave is therefore determined by the angle δ, and the width of the emission feature by the opening angle of the cone. (We have chosen parameters which roughly match the WR 139 observations shown in Fig. 8.)

For $i = 90°$, the line of sight coincides with the axis of symmetry of the cone at two phases, $\delta/360°$ and $(\delta + 180°)/360°$ (i.e., phases 0.125 and 0.625 in our model), when the projected velocity is the identical for all points on the shock surface. The shock emission is therefore concentrated at one point in the observed line profile at these two phases, giving rise to sharp features in the model spectra. These match the phase-dependent appearance of the brightest points in the observed spectra reasonably well.

In practice, the projected velocities do not converge precisely on a single value for the model, because the shock cone actually has a somewhat curved surface, because there is a small velocity dispersion in calculated shock velocities, and because the axis of symmetry does not pass through the system centre of mass. In real systems, these effects will be further complicated by 'wrap-round' of the shock surface resulting from binary rotation. None the less, it is clear that the extra emission from the shocked region gives a good general match to the observed line-profile variability, and is likely to be the dominant factor in that variability.

4.4 Discussion

Our models, and associated interpretation of the observations, appear to be successful in accounting for at least the gross characteristics of the He I 1.0830-μm emission we have observed, and in particular emphasize the importance of line emission from the wind–wind interface. They also allow us to develop a general understanding of the expected level of variability in different WR + O-star binaries. In long-period systems we expect generally smaller effects, for two reasons. First, in wide systems the post-shock gas is unlikely to cool efficiently, and hence will remain too hot for substantial localized He I 1.0830-μm emission from the wind–wind interface. Secondly, if the binary separation is greater than the He I 1.0830-μm line-formation region, the presence of the O star and its wind will make little difference to the observed line profile. In systems where there is a very large momentum ratio, $\mathcal{R}$, the effect of the companion will also be smaller, at least as far as generating a cavity in the distributed emission is concerned.

We can also speculate on how colliding-wind models may relate to observations of P Cygni absorption components. For most of the systems we observed, that absorption weakens around at around phase 0.5–0.6. At these phases the line-of-sight passes close to or through the O-star wind (i.e., the He I cavity). Consequently, we would expect a reduction in absorption by the high-velocity WR wind, at $\phi \simeq 0.5$ in the absence of rotational distortion and at progressively later phases as the importance of rotation increases.

One shortcoming of our models is that they fail to reproduce the excess emission observed outside of the general S-wave pattern, clearly present in the difference-spectrum grey-scales for both WR 139 and, slightly less strongly, WR 153 (Figs 2 and 3). That emission appears as a high-velocity blue-shifted feature from $\phi \sim 0.7$, and is strong until $\phi \sim 1.0$, when it disappears rather abruptly ($\Delta\phi \ll 0.1$); analogous behaviour occurs in the red wing for $\phi \sim 0.2$–0.5. The origin of these two high-velocity features is problematic, as there is no obvious site of emission with the necessary dynamical characteristics, although the rather rapid disappearance may suggest some sort of occultation mechanism, and hence, perhaps, a small region of emission rather close to the O-type component.

An alternative interpretation is that these effects are a consequence of failing to compensate for orbital motion in constructing the difference spectra, since subtracting a fixed mean spectrum from a profile which follows the orbital motion of the WR component will generate features in the grey-scale roughly similar to those observed. We might expect the wind lines to follow the orbital motion, since the wind flow time across the binary separation is much shorter than the orbital period (by a factor of ∼20 in the case of V444 Cyg), but in practice it appears that the λ1.0830-μm line does *not* follow the WR orbit (see, e.g., the left-hand grey-scale in Fig. 2). Although there may be some contribution to the high-velocity features from this mechanism, simply correcting for orbital motion results in a grey-scale that is completely dominated by the reflex response of the velocity corrections applied.

In summary, we have presented new observations showing large-scale, orbital line-profile variability in WR binaries. The observations show that He I 1.0830-μm is an excellent tracer of circumstellar material and interacting winds in WR+O-star systems. Our simple models show that much (though not all) of the systematic variability can be understood in terms of a standard colliding-wind paradigm, and emphasize that the He I 1.0830-μm line is a potentially potent diagnostic of the distribution of post-shock gas.

ACKNOWLEDGMENTS

IRS acknowledges PPARC funding. Data reduction and modelling were carried out using facilities provided by the Starlink Project, which is run by CCLRC on behalf of PPARC. At the time of the observations, the Isaac Newton Telescope was operated on the

island of La Palma by the Royal Greenwich Observatory in the Spanish Observatorio del Roque de los Muchachos of the Instituto de Astrofisica de Canaries. We thank Jenny MacDonald for help with the 1992 observations, and Werner Schmutz for his collaboration in the 1990 observing. Paul Crowther, Mark Jex and Malcolm Fairbairn helped with the analysis, and Sergey Marchenko made a number of helpful comments and suggestions on the first version of this paper.

REFERENCES

Aslanov A. A., Cherepashchuk A. M., 1981, SvA Lett., 7, 265
Cherepashchuk A. M., 1976, SvA Lett., 2, 138
Cherepashchuk A. M., 1982, Ap&SS, 86, 299
Conti P. S., Howarth I. D., 1998, MNRAS, in press
Corcoran M. F., Stevens I. R., Pollock A. M. T., Swank J. H., Shore S. N., Rawley G. L., 1996, ApJ, 464, 434
Eenens P. R. J., Williams P. M., 1994, MNRAS, 269, 1082
ESA, 1997, The Hipparcos and Tycho Catalogues, Hipparcos Epoch Photometry Annex (ESA-SP1200)
Gayley K. G., Owocki S. P., Cranmer S. R., 1997, ApJ, 475, 786
Grandchamps A., Moffat A. F. J., 1991, in van der Hucht K. A., Hidayat B., eds, Wolf–Rayet Stars and Interrelations with Other Massive Stars in Galaxies. Kluwer, Dordrecht, p. 258
Hamann W.-R., Schwarz E., 1992, A&A, 261, 523
Harries T. J., Hilditch R. W., 1997, MNRAS, 291, 544
Harries T. J., Hillier D. J., Howarth I. D., 1998, MNRAS, 296, 1072
Hillier D. J., 1987, ApJS, 63, 947
Hillier D. J., Kudritzki R. P., Pauldrach A. W., Baade D., Cassinelli J. P., Puls J., Schmitt J. H. M. M., 1993, A&A, 276, 117
Hiltner W. A., 1945, ApJ, 101, 356
Hjellming R. M., Hiltner W. A., 1963, ApJ, 137, 1080
Howarth I. D., Schmutz W., 1992, A&A, 261, 503
Howarth I. D., Willis A. J., Stickland D. J., 1982, in Proc. 3rd European IUE Conf. (ESA SP-176), p. 331
Howarth I. D., Murray J., Mills D., Berry D. S., 1996, DIPSO – a friendly spectrum analysis program (Starlink User Note 50). CCLRC/Rutherford Appleton Laboratory
Khaliullin Kh. F., Khaliullina A. I., Cherepashchuk A. M., 1984, SvA Lett., 10, 250
Kilinç B., 1994, Inf. Bull. Variable Stars No. 3998
Koenigsberger G., Firmani C., Bisiacchi G. F., 1980, Rev. Mex. Astron. Astrofis., 5, 45
Lewis D., Moffat A. F. J., Matthews J. M., Robert C., Marchenko S. V., 1993, ApJ, 405, 312
Lührs S., 1995, in van der Hucht K. A., Williams P. M., eds, Wolf–Rayet Stars: Binaries, Colliding Winds, Evolution. Kluwer, Dordrecht, p. 416
Luo D., McCray R., Mac Low M.-M., 1990, ApJ, 362, 267
Marchenko S. V., Moffat A. F. J., Koenigsberger G., 1994, ApJ, 422, 810
Marchenko S. V., Moffat A. F. J., Eenens P. R. J., Hill G. M., Grandchamps A., 1995, ApJ, 450, 811
Marchenko S. V., Moffat A. F. J., Eenens P. R. J., Cardona O., Echevarria J., Hervieux Y., 1997, ApJ, 485, 826
Marchenko S. V. et al., 1998, A&A, 331, 1022
Massey P., 1981, ApJ, 244, 157
Massey P., Grove K., 1989, ApJ, 344, 870
Massey P., Niemela V. S., 1981, ApJ, 245, 195
Matthews J. A., Beech M., 1987, ApJ, 313, L25
Mills D., Webb J., Clayton M., 1997, ECHOMOP – Echelle Data Reduction Package (Starlink User Note 152). CCLRC/Rutherford Appleton Laboratory
Panov K. P., Seggewiss W., 1990, A&A, 227, 117
Pollock A. M. T., Haberl F., Corcoran M. F., 1995, in van der Hucht K. A., Williams P. M., eds, Wolf–Rayet Stars: Binaries, Colliding Winds, Evolution. Kluwer, Dordrecht, p. 512
Prilutskii O., Usov V. V., 1976, SvA, 20, 2
Robert C., 1994, Ap&SS, 221, 137
Schmutz W., Hamann W.-R., Wessolowski U., 1989, A&A, 210, 236
Shore S. N., Brown D. N., 1988, ApJ, 334, 1021
Shortridge K., Meyerdierks H., Currie M., Clayton M., Lockley J., 1997, FIGARO: a general data reduction system (Starlink User Note 86). CCLRC/Rutherford Appleton Laboratory
Stevens I. R., 1993, ApJ, 404, 281
Stevens I. R., Pollock A. M. T., 1994, MNRAS, 269, 226
Stevens I. R., Blondin J. M., Pollock A. M. T., 1992, ApJ, 386, 265
Stickland D. J., Bromage G. E., Budding E., Burton W. M., Howarth I. D., Jameson R., Sherrington M. R., Willis A. J., 1984, A&A, 134, 45
St-Louis N., Smith L. J., Stevens I. R., Willis A. J., Garmany C. D., Conti P. S., 1989, A&A, 226, 249
St-Louis N., Moffat A. F. J., Lapointe L., Efimov Yu. S., Shakhovsky N. M., Fox G. K., Piirola V., 1993a, ApJ, 410, 342
St-Louis N., Willis A. J., Stevens I. R., 1993b, ApJ, 415, 298
Underhill A. B., Yang S., Hill G. M., 1988, PASP, 100, 741
Underhill A. B., Grieve G. R., Louth H., 1990, PASP, 102, 749
van der Hucht K. A., Hidayat B., Admiranto A. G., Supelli K. R., Doom C., 1988, A&A, 199, 217
Vreux J.-M., Andrillat Y., Gosset E., 1985, A&A, 149, 337
Vreux J.-M., Andrillat Y., Biémont E., 1990, A&A, 238, 207
Walker E. N., Lloyd C., Pike C. D., Stickland D. J., Zuiderwijk E. J., 1983, A&A, 128, 394
Williams P. M., Eenens P. R. J., 1989, MNRAS, 240, 445
Williams P. M., van der Hucht K. A., Pollock A. M. T., Florkowski D. R., van der Woerd H., Wamsteker W. M., 1990, MNRAS, 243, 662
Williams P. M., van der Hucht K. A., Bouchet P., Spoelstra T. A. Th., Eenens P. R. J., Geballe T. R., Kidger M. R., Churchwell E., 1992, MNRAS, 258, 461
Williams P. M., Dougherty S. M., Davis R. J., van der Hucht K. A., Bode M. F., Setia Gunawan D. Y. A., 1997, MNRAS, 289, 10
Willis A. J., Schild H., Stevens I. R., 1995, A&A, 298, 549
Wilson O. C., 1940, PASP, 52, 404
Wrigge M., Wendker H. J., Wisotski L., 1994, A&A, 286, 219

This paper has been typeset from a TEX/LATEX file prepared by the author.